Energy dependence of proton induced fission cross sections for heavy nuclei in the energy range 200–1000 MeV

A. A. Kotov, L. A. Vaishnene, V. G. Vovchenko, Yu. A. Gavrikov, V. V. Poliakov, M. G. Tverskoy, O. Ya. Fedorov, Yu. A. Chestnov, A. I. Shchetkovskiy, and A. V. Shvedchikov
Petersburg Nuclear Physics Institute, RU-188300 Gatchina Leningrad District, Russia

A. Yu. Doroshenko
SSC Institute of Physics and Power Engineering, RU-249020 Obninsk, Kaluga Region, Bondarenko Sq. 1, Russia

T. Fukahori
Japan Atomic Energy Research Agency, Tokai-mura, Ibaraki-ken 319-1195, Japan
(Received 30 December 2005; published 27 September 2006)

Total cross sections for proton induced fission of ^{nat}Pb, ^{209}Bi, ^{232}Th, ^{233}U, ^{235}U, ^{238}U, ^{237}Np, and ^{239}Pu nuclei were measured in the range 200–1000 MeV with an energy step of 100 MeV. The experiment was carried out at 1 GeV in a PNPI synchrocyclotron. Complementary fragments of the binary fission from a thin target were detected in coincidence by two parallel plate avalanche counters (PPAC) located close to the target. An assembly of the two PPACs and with the target in between them was placed directly into the beam, which provided a large solid angle acceptance. The beam monitoring system employed a scintillation counter telescope that was used for direct proton counting as well as for registration of the elastic *pp*-scattering events from the auxiliary $(CH_2)_n$ target. The measured energy dependence of the total fission cross sections is presented. The results are compared with other available experimental data as well as with calculations in the frame of the cascade-evaporation model.

DOI: 10.1103/PhysRevC.74.034605 PACS number(s): 25.85.Ge, 24.75.+i, 27.90.+b

I. INTRODUCTION

The need for data on the fission of heavy nuclei has existed for a long time and is still topical. The interest in the data stems from both fundamental and applied applications of nuclear physics. However, despite considerable experimental and theoretical efforts aimed at the understanding of the fission process, many details of the proces's mechanism are still unclear. One should note that after many years since the discovery of binary fission there exists no theory adequate to describe the characteristics of the fission process for a broad range of fissioning nuclei within a wide range of projectile energy. Measurement of the energy dependence of total fission cross sections for heavy nuclei would give new insights into both the fission process and the mechanism of the nucleon interaction with the nucleus. In addition, it could provide information on the properties of highly excited nuclei, such as the temperature dependence of the level density and of the fission barriers.

The most important applied problems are energy production techniques based on accelerator driven systems, nuclear waste transmutation technologies, and radiation shield designs for accelerators and cosmic devices [1]. All these problems require the total fission cross sections to be known with high accuracy and reliability in a wide proton energy range.

At low proton energies (from the threshold to ∼150 MeV) a considerable amount of experimental data demonstrates unambiguously the sharp rise of the fission cross sections for actinide nuclei up to the maximum at several tens of MeV, followed by a decrease. However, for higher proton energies the data are quite fragmentary and contradictory; for ^{239}Pu and ^{233}U nuclei data are practically absent. As for the pre-actinide nuclei ^{nat}Pb and ^{209}Bi, in the energy range in question data are very scarce and are absent in the range from 600 to 1000 MeV.

Measurement of total fission cross sections is not simple. The main difficulty here is to reliably detect the fission process against the background of other nuclear reactions that accompany the fission. The majority of the available data on fission cross sections was obtained in experiments that employed various methods of detection of the fission fragments. In most of experiments the threshold technique was used to detect only one of the fission fragments, which did not allow reliable detection of the fission process from other nuclear reactions. For this reason the available data for energies >200 MeV vary considerably, differing from each other far beyond the errors presented, and do not allow unambiguous estimation of the energy dependence of fission cross sections [2,3]. The reliable and accurate measurement of fission cross sections is possible only with up-to-date high aperture electronic techniques, providing detection of both fission fragments in coincidence as well as measurement of their kinetic energies [4]. Only such methods with amplitude analysis of the detection signal can provide a reliable selection of the fission events and minimize possible measurement errors. In the present experiment method of detection of two fission fragments in coincidence by two parallel plate avalanche counters (PPAC) was used. Insensitivity of the PPAC to light charged particles allowed us to locate the assembly with the two PPACs with the target in between them directly

into the proton beam, which provided a large solid angle for the fragment detection. A special monitoring procedure was used based on direct proton counting by a telescope of thin scintillation counters. The method used allowed us to measure the total proton induced fission cross sections for ^{nat}Pb, ^{209}Bi, ^{232}Th, ^{233}U, ^{235}U, ^{238}U, ^{237}Np, and ^{239}Pu nuclei in the energy range of 200 to 1000 MeV with an energy step of 100 MeV at a rather low proton beam intensity of 10^5 to 10^7 s^{-1}.

II. EXPERIMENT

The experiment was performed at 1 GeV in the synchrocyclotron at the Petersburg Nuclear Physics Institute. Thin targets of the mentioned isotopes were irradiated by protons and the binary fission fragments were detected in coincidence by the two PPACs. The proton flux at the target was measured by direct counting of protons with a scintillation counter telescope, as well as with the help of a secondary monitor, and by counting the elastic pp-scattering events from a polyethylene target. Knowing the number of binary fission events, the number of protons that passed through the target, the solid angle for the fragment detection, and the number of nuclei in the target, one can obtain the total cross section by

$$\sigma_f = \frac{2\pi Y_f}{N_p \Omega_{\text{det}} T},$$

where Y_f is the number of the fission events, N_p is the number of protons, Ω_{det} is the solid angle of the detection (steradian), and T is the target thickness (atoms/cm^2).

A. Proton beams

Because the external proton beam of the PNPI synchrocyclotron has a fixed energy of 1 GeV, to obtain proton beams with energies in the range of 900 to 200 MeV a method of decreasing energy by beam absorption in a copper degrader was applied [5]. The absorption processes in the degrader were first analyzed with a GEANT-3 simulation code [6]. The calculations showed that even at the proton energy of 200 MeV one could obtain a beam intensity at the degrader outlet of up to $4 \cdot 10^7$ s^{-1}, which was sufficient for the experiment planned.

The system of beam transport from the degrader outlet to the fragment detection chamber was designed on the basis of beam optics calculations and is shown in Fig. 1. The system comprised two quadrupole doublets (ML1, ML2), a bending magnet (BM), and collimators C1–C3. The collimators C1 and C2, located after the degrader (D), served to narrow the secondary beam dimensions and angular divergency before the magneto-optical system. After the first doublet, ML1, the proton beam was rotated by 18° with the BM and then went through the C3 collimator, which was 3 m in length and 100 mm in diameter, located in the shielding wall. The second doublet, ML2, was placed just before the experimental setup and served to focus the beam onto the target. In fact the system for beam transport and formation was a kind of magnetic spectrometer with a high resolution of $\Delta p/p \approx 0.008$ (FWHM). The beam characteristics were determined from a series of measurements and agreed with the Monte-Carlo calculations [5]. The intensity measurements showed that even for 200-MeV protons one could achieve an intensity of 10^7 s^{-1} at the 2×2 cm^2 area, which was quite enough for the experiment.

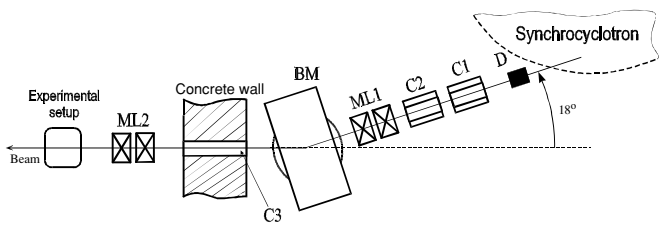

FIG. 1. System of beam transport. D, copper degrader; BM, bending magnet; C1, C2, C3, A collimators; ML1, ML2, quadrupole doublets.

Proton energy was measured by the time-of-flight (TOF) method. Proton energy after the degrader was found to have normal distribution; its relative width (FWHM/E) was maximal at beam energies of 200 and 300 MeV and did not exceed 7%. The TOF spectra analysis showed that the π^+ mesons were practically absent.

The beam diameter at the target chamber location for all proton energies did not exceed 40 mm. The beam profile was measured by a thin scintillation counter that scanned the beam in two orthogonal directions. The beam divergency was determined by measuring the beam profile at the chamber's inlet, outlet, and center, at each proton energy variation. The beam intensity distribution at the target was a bidimensional normal distribution with the FWHM not larger than $\sim$ 18 mm.

B. Layout of the device used for fission event detection

One particular characteristic of fission fragment detection is connected with high specific energy losses of the fragments. This means that the target must be thin enough, which makes the experiment rather time consuming, especially for pre-actinide nuclei and for measurements in a distant geometry, when fission fragment detectors are located beyond the beam of the projectiles. Therefore, it is quite reasonable to employ the large solid-angle technique for fragment detection, which allows one to locate the detectors together with the target directly into the beam. Among such methods one could mention a nuclear emulsion method, a radiochemical method, and a "sandwich" method, in which solid-state detectors and thin film breakdown counters are used [7]. The majority of these methods do not provide, however, a sufficient number of selection criteria to reliably isolate the fission events from the bulk of background events, induced by the projectiles in the target and in the detector material. In the present experiment gas PPACs were used as fragment detectors because they have high efficiency for fragment detection and good time characteristics (better than 300-ps time resolution for fission fragments). The latter property, together with their insensitivity to neutrons, photons, and light charged particles with minimal energy loss in the matter, makes PPACs an extremely favorable tool for accelerator experiments because they can be placed in

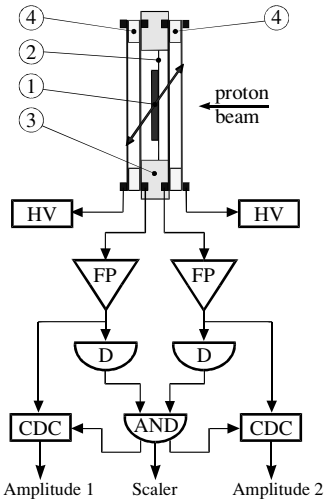

FIG. 2. Schematic drawing of the method of fission fragment registration. 1, target; 2, backing; 3, target support; 4, PPAC; HV, high voltage; FP, fast amplifier; D, discriminator; AND, coincidence unit; CDC, charge-to-digital converter.

the direct proton beam, which provides the large solid angle necessary for fragment registration [8].

In the present experiment the fission fragment detector comprised an assembly of two identical PPACs with the target to be studied located between the two PPACs in Fig. 2. The working gap between the PPAC electrodes was 1 mm. The electrodes were made of 2-μm-thick aluminized Mylar and were 84 mm in diameter. To eliminate edge effects, a collimator of 80 mm in diameter was placed just before each PPAC. Heptane vapor at 6–10 Torr was used as the working gas.

The PPAC pulse amplitude is determined by both the specific energy losses of the detected particles in heptane and the gas amplification value. The latter depends on the voltage value between the anode and the cathode; therefore, detection efficiency can be controlled by voltage choice. The dependence of fragment detection efficiency on the voltage was previously measured for each PPAC using the source of spontaneously fissioning ^{252}Cf isotope.

The counting rate for one of the PPACs is shown in Fig. 3 as a function of the cathode voltage. Two plateaus are clearly seen. The first one, above 450 V, corresponds to the full-scale efficiency (100%) for fission fragment detection. The second one, which begins at 615 V, corresponds to the full-scale detection efficiency for both fission fragments and α particles. Such a characteristic allows one to introduce a threshold selection criterion that is especially important when detecting the fission fragments from the nuclei with high levels of α activity, such as ^{233}U, ^{237}Np, and ^{239}Pu.

Nevertheless, it is not sufficient to employ only the threshold selection criterion when using the PPACs directly in the proton beam. In fact, the amplitude spectrum of the detected particles contains, together with the fission fragments, a considerable contribution of low-amplitude background events. These events are caused by various proton induced nuclear reactions in the matter along the beam line. Such a low-energy component is strongly suppressed after a coincidence criterion is switched on. In the real experiment its contribution

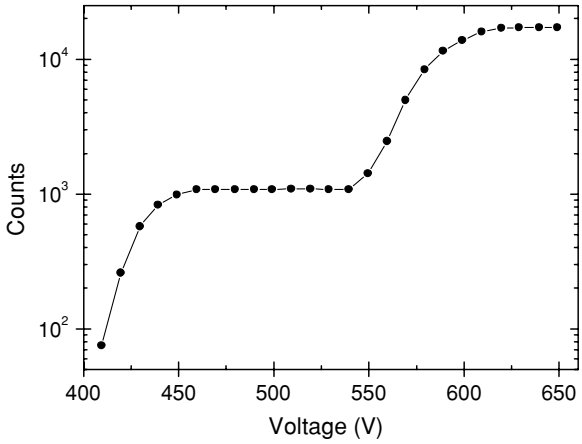

FIG. 3. Registration efficiency of the PPAC for fission fragments of ^{252}Cf versus the anode-cathode potential.

did not exceed 2–3%. Moreover, the analysis of amplitude correlations of the coinciding fragments allowed us to exclude all background events almost thoroughly. This is clearly seen in Fig. 4, where the bidimensional amplitude distribution of the coinciding events is shown for the ^{238}U target and 1-GeV proton beam. The distribution over the sum of the amplitudes is also shown.

Thus, in our experiment we used three criteria to select the binary fission events: threshold criterion, coincidences, and the

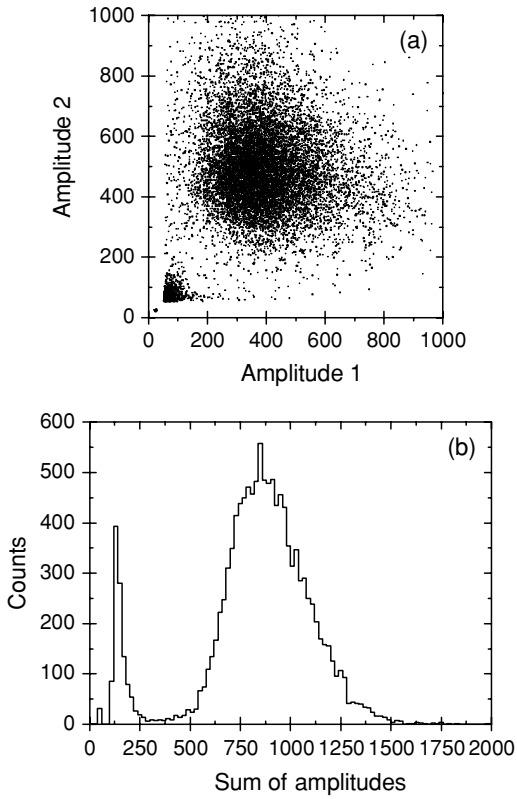

FIG. 4. (a) Amplitude scatter plot of fission events for the uranium target. (b) Distribution over the sum of the amplitudes.

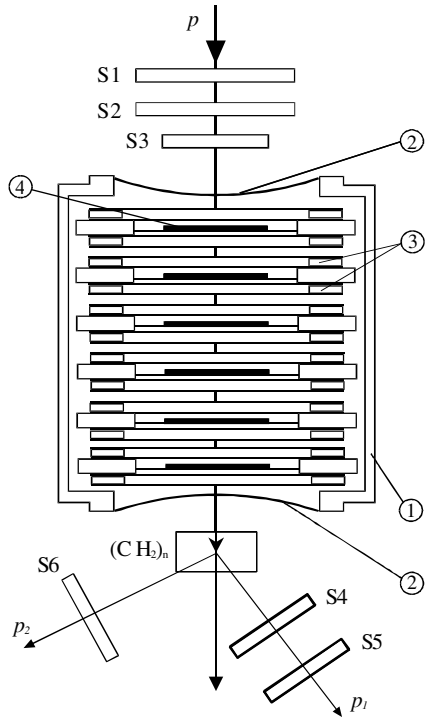

FIG. 5. Experimental setup. 1, chamber filled by heptane; 2, entrance window; 3, PPACs; 4, target; S1, S2, S3, S4, S5, and S6 scintillation counters.

criterion of the total kinetic energy of the detected coincident particles (the amplitude correlations).

The PPAC is so thin that it does not harm practically the beam characteristics when located in the beam. For this reason several assemblies with various targets could be readily placed in the beam. This allowed us to diminish considerably the measurement time. In the real experiment up to six assemblies were used at a time. To exclude thoroughly the possibility of registration of the particles coming from neighboring α-active targets, all assemblies were separated by 20-μm Mylar films. The layout of the setup including the reaction chamber with the fission event detectors and the proton monitoring system is shown in Fig. 5. The scheme of the electronics is shown in Fig. 6.

The main part of the setup is a hermetic chamber with six detector assemblies. Each assembly comprises the two PPACs and a target placed in between them. After it was vacuum pumped out, the chamber was filled with *n*-heptane vapor. Before entering the reaction chamber the proton beam passed three scintillation counters (S1&S2&S3), combined via the coincidence scheme, and direct proton counting was performed. The scintillators of the S1 and S2 counters were 80 mm in diameter, whereas the S3 scintillator, placed just in front of the reaction chamber, was 40 mm in diameter, which provided the total overlap of the proton beam. The proton beam then entered the reaction chamber through 80-μm-thick Capton windows. Just downstream of the reaction chamber the polyethylene target $(CH_2)_n$ was placed. The protons elastically scattered from this target were detected by a two-arm scintillation telescope (S4&S5&S6), which served as a secondary beam monitor.

The signals from each PPAC were amplified by fast preamplifiers (FP) and then sent on to the inlet of pulse shapers (D). The analog signals from the linear outlets (A) of the pulse shapers after additional amplification (FA) and corresponding delay were then sent on to the inlet channels of the charge-code converter (CDC). At the same time, logical signals (L) from the shapers corresponding to each PPAC assembly entered in pairs the corresponding coincidence units "AND." Signals from each coincidence unit entered the input register, which fixed the number of the assembly fired, as well as the "OR" unit, whose outlet signal started the gate generator. The latter produced a signal to launch the CDC as well as a stop signal for the time-to-digit converter (TDC), which served to measure the time distribution of the fission events with respect to the start signal, corresponding to the beginning of the proton beam extraction. The event registration system was started by a pulse from the gate generator, coming at the input register, which, in turn, produced the "look at me" (LAM) signal. The LAM signal caused the data processing code to read out the amplitude PPAC signals (from the CDC), the number of the assembly fired (input register), the time of event with respect to the start moment of the proton beam extraction (TDC), and the information from all the scalers, which detected the number of protons (S1&S2&S3), the number of the elastic *pp*-scattering events (S4&S5&S6), and the counting loads of all the PPACs and scintillation counters.

C. Proton beam monitoring

Direct counting of the incident protons with a scintillation counter telescope was used for beam monitoring. This method provides good monitoring accuracy only for low-intensity beams, up to $\sim 10^5$ s^{-1}, because of the beam time structure. This structure is determined by the extraction system of the 1-GeV proton beam and represents a sequence of macropulses with a frequency of $\sim$45–50 Hz and a duration of $\sim$8–10μs. Each macropulse, in turn, comprises microbunches of $\sim$10 ns in duration going with the period of $\sim$74 ns. For such a short microbunch it is not possible to detect more than one proton in a microbunch. It is clear that the reliability of monitoring is connected with the probability of the appearance of more than one proton in a microbunch, which depends strongly on the proton beam intensity. It can be shown [9] that for intensity $< 10^5$ s^{-1} such a probability does not exceed 1.1%. This value determines, in fact, the correction value for the intensity, measured by the beam monitor. Experimentally the correction for the false counts, caused by the appearance of more than one proton in a microbunch, was measured by counting the delayed coincidences, i.e., the number of monitor counts caused by coincidences of protons from the two neighboring microbunches. It was found that direct proton counting is a good monitoring method (with a false count correction $< 3\%$) only for beam intensities not higher than $3 \cdot 10^5$ s^{-1} [9]. To obtain the efficiency of the proton detection by the telescope (S1&S2&S3) we registered the coincidence of the fission event in one of the targets with the proton signal from the telescope, corresponding to the proton that

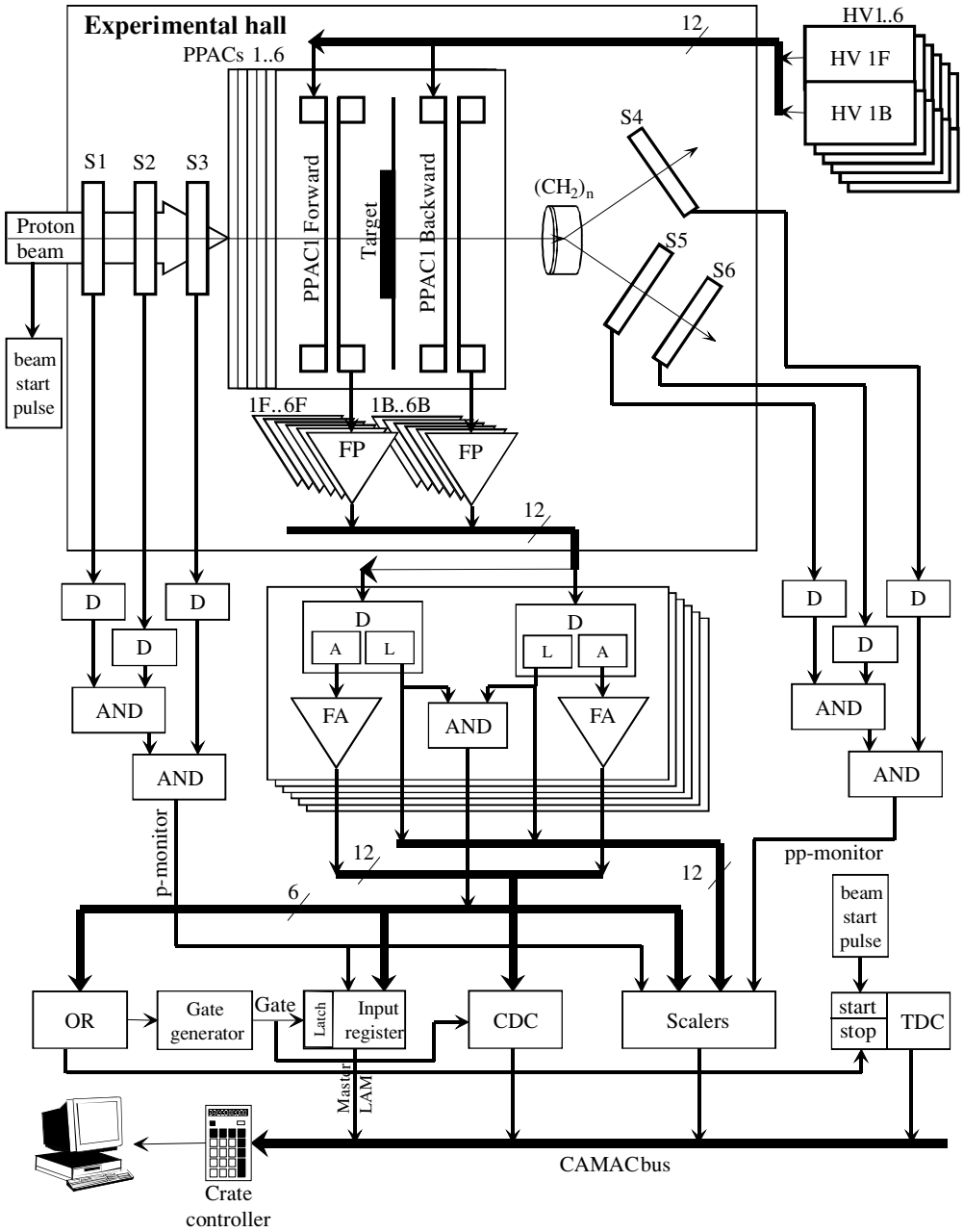

FIG. 6. Electronic scheme.

caused the fission. Taking into account almost 100% efficiency of the fission fragment detection by the PPAC, the efficiency of the telescope was determined by the ratio of the number of fission events accompanied by the telescope signal to the total number of fission events. The measured correction value for the telescope efficiency did not exceed 5%–7%.

The data taking rate for the uranium target of $179\mu g/cm^2$ at a proton beam intensity of 10^5 s^{-1} amounted to $\sim$10 events per minute. Such a rate allowed us to provide the necessary statistical accuracy for the actinide nuclei within a reasonable amount of time. However, for pre-actinide bismuth and lead nuclei with fissility about an order of magnitude lower, one needs much higher intensity. For this reason the measurements were performed at two intensity values of the proton beam: $\sim 10^5$ s^{-1} and 10^6–10^7 s^{-1}. In the latter high-intensity case the beam monitoring was done by two methods: (i) by detection of the fission events from the calibration target of ^{238}U, residing in the reaction chamber, and (ii) by detecting the events of the *pp*-scattering on the auxiliary $(CH_2)_n$ target with the two-arm scintillation telescope (S4&S5&S6). Both methods were previously calibrated at low intensity ($<2 \cdot 10^5$ s^{-1}) with the direct monitoring telescope (S1&S2&S3). The comparison of both methods at high intensity showed the agreement of the results within $\sim$3% at all energies from 200 to 1000 MeV. The calibration procedure for secondary monitoring is described in detail in Ref. [9].

D. Targets

The target to be investigated was a thin layer of material laid by vacuum evaporation on a thin (50 mm in diameter) backing foil made of alumina (Al_2O_3). The target diameter was 40 mm. Fluorides and oxides of the isotopes were used to prepare actinide targets. The lead target contained the natural mixture of isotopes. The thickness of actinide targets, their composition, and the uniformity of the evaporated layer were determined by measuring the α activity and the energy spectra of the α particles, the α-particle detection being performed with the PPAC and the surface-barrier Si(Au) detector. The energy resolution of the spectrometric channel amounted to ~50 keV, which allowed us to determine reliably the isotope contents of the target. The uniformity of the target thickness was determined by measuring the α activity at several points on the target, fixed by collimators, and turned out to be not worse than 96%.

For the lead and bismuth targets the thickness of the backings and targets was determined by measuring energy losses of α particles when passing through the target; the range-energy tables of Refs. [10,11] were used. As for the target composition, the maximum admixture value for the actinide targets (except ^{239}Pu) did not exceed 0.01%. For the ^{239}Pu target the main admixture was the spontaneously fissioning ^{238}Pu isotope, whose admixture amounted to ~4%. The characteristics of the targets and backings are presented in Table I.

III. RESULTS

Using the methods of detection of binary fission events and beam monitoring described in the previous sections, we measured the fission cross sections for each target at nine proton energies. At each energy the measurement was performed for two intensity levels of the proton beam, low (~10^5 s^{-1}) and high (~10^6–10^7 s^{-1}).

At low intensity the beam profile at the target was measured and normalization of the secondary beam monitors [i.e., fission event counting from the calibration ^{238}U target and elastic *pp*-scattering event registration from the $(CH_2)_n$ target] upon the fixed number of protons passed through the chamber was performed. The measurement time period was determined by the number of detected fission events from the calibration ^{238}U target, which provided the statistical accuracy of <2%. At the same time the number of *pp*-scattering events was not less than $3\cdot10^4$. Then at high intensity the data taking run was carried out to obtain the resulting statistical accuracy of not worse than 1%–2% for each target.

TABLE I. Target characteristics.

Target	Thickness (μg/cm^2)	Nonhomogeneity (%)	Backing thickness (μg/cm^2)
^{nat}Pb	465 ± 19	<1.2	69 ± 2
^{209}Bi	228 ± 13	<4	47 ± 4
^{232}Th	93 ± 3	<1.5	82 ± 2
^{232}Th	72 ± 3	<1.5	80 ± 2
^{233}U	77 ± 4	<1.7	72 ± 2
^{235}U	110 ± 6	<3.7	60 ± 4
^{238}U	179 ± 6	<1.7	85 ± 2
^{237}Np	144 ± 6	<1.5	94 ± 4
^{239}Pu	106 ± 6	<1.5	75 ± 4

The cross section calculation procedure comprised the following steps.

(i) Background subtraction after analysis of the bidimensional amplitude distribution of the detected events. The number of background events amounted to 2%–3% of the total number of the detected events.

(ii) Determination of the solid angle for fission event detection for each assembly. The calculation was carried out using a Monte-Carlo simulation that took into account the following: the proton beam profile at the target, the detection geometry for the fission fragments and their mass and energy distributions, and the anisotropy of fragment angular distribution in the laboratory system due to the longitudinal momentum component of the fissioning nucleus. The mass and energy distributions were taken from the experimental data for uranium and bismuth nuclei at proton energies of 156 MeV [12] and 1 GeV [13]. The distribution in the longitudinal component of the momentum transfer was obtained from experimental angular correlations for uranium and bismuth nuclei at energies of 156 MeV [14,15] and 1 GeV [16], as well as for ^{232}Th nuclei in the energy range 140–1000 MeV [17]. The statistical accuracy of the solid angle calculations amounted to 0.1%.

(iii) Estimation of the undetectable portion of the fission events, caused by the energy loss of the fission fragment in the target and its backing and in the PPAC electrodes. The energy losses were calculated for the whole spectrum of coinciding fission fragments, which was obtained using the Monte-Carlo calculations with the help of the SRIM code [10]. The undetectable part of the events depended on the target nucleus and thickness and amounted to 3%–8%.

(iv) Determination of the integral proton flux through the target, with the account of the scintillation telescope efficiency and the probability of the appearance of more than one proton in a microbunch at low intensity. Determination of the normalizing coefficients to calculate the proton flux at high intensity via the counting rate of the *pp*-scattering monitor and the fission counting rate from the calibration target.

The measured fission cross sections for ^{239}Pu, ^{237}Np, ^{233,235,238}U, ^{232}Th, ^{209}Bi, and ^{nat}Pb nuclei are shown in Table II. For most of the nuclei the data presented are the average of the results of several measurements, the errors being determined mainly by the monitoring errors and the uncertainty in the target thickness. The energy dependence of the fission cross sections obtained in the present experiment for the mentioned nuclei is shown in Figs. 7–14.

The results of the previous experiments, compiled in Refs. [2,3], are also given. In Figs. 7–14 the data from compilations

TABLE II. Fission cross sections (mbarn).

Energy (MeV)	^{239}Pu	^{237}Np	^{238}U	^{235}U
207	1260 ± 126	1187 ± 81	1352 ± 68	1464 ± 83
302	1339 ± 134	1438 ± 98	1470 ± 68	1562 ± 94
404	1585 ± 158	1624 ± 88	1527 ± 104	1626 ± 138
505	1613 ± 161	1607 ± 98	1491 ± 78	1592 ± 102
612	1628 ± 163	1647 ± 100	1499 ± 72	1610 ± 124
702	1700 ± 170	1674 ± 102	1518 ± 76	1620 ± 131
802	1672 ± 167	1629 ± 88	1503 ± 63	1571 ± 90
899	1688 ± 168	1673 ± 114	1490 ± 63	1592 ± 96
1000	1592 ± 159	1568 ± 96	1489 ± 64	1591 ± 113
Energy (MeV)	^{233}U	^{232}Th	^{209}Bi	$^{(nat)}$Pb
207	1625 ± 162	1144 ± 90	136 ± 13	60.5 ± 3.5
302	1651 ± 115	1200 ± 91	178 ± 17	84 ± 4.5
404	1767 ± 124	1236 ± 91	207 ± 21	110 ± 6
505	1818 ± 123	1239 ± 61	227 ± 23	118.5 ± 6
612	1763 ± 123	1268 ± 80	233 ± 23	127 ± 6.5
702	1798 ± 126	1285 ± 81	235 ± 23	132.5 ± 9.5
802	1778 ± 124	1247 ± 54	229 ± 23	131 ± 8.5
899	1779 ± 122	1252 ± 58	239 ± 24	133.5 ± 7.5
1000	1745 ± 122	1245 ± 85	235 ± 23	129 ± 8.5

[2,3] were supplemented by the data on the fission of ^{237}Np, ^{235,238}U, ^{232}Th, and ^{209}Bi nuclei induced by 1000-MeV protons [18].

In Ref. [2], a parametrization of all the world fission cross section data was proposed after the critical analysis and data selection for the actinide and pre-actinide nuclei for proton energies up to 10–30 GeV. The results of this cross section estimation based on all the world experimental data are also shown in Figs. 7–14 by dashed lines.

As seen from Figs. 7–12 the energy dependence of the fission cross sections for all actinide nuclei is characterized by common regularities, demonstrating the rise of the cross sections in the energy range 200 to 400 MeV with a subsequent plateau up to 1000 MeV. Such behavior is not consistent with estimations of Ref. [2] (dashed lines), which predict smooth decreases of the cross sections with energy in the range 200–1000 MeV.

Only for ^{237}Np, ^{238}U, ^{235}U, and ^{232}Th nuclei one can compare our results with the data of previous experiments, because for ^{239}Pu (Fig. 7) and ^{233}U (Fig. 11) the data in the range 200–1000 MeV are absent.

For the ^{237}Np target our data (Fig. 8) are in a good agreement with the results of previous experiments in the range 300–1000 MeV, though at 200 MeV our cross section value lies somewhat lower.

For ^{238}U, ^{235}U, and ^{232}Th (Figs. 9, 10, and 12) the situation is different. For ^{238}U and ^{235}U the agreement is satisfactory only

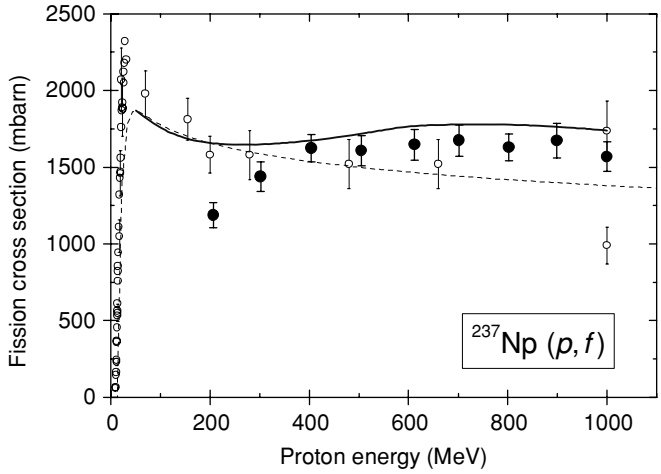

FIG. 8. Energy dependence of fission cross sections for ^{237}Np. Solid circles, our data; open circles, data from Refs. [2,3]; dashed line, a parametrization from Ref. [2]; solid line, theoretical calculation.

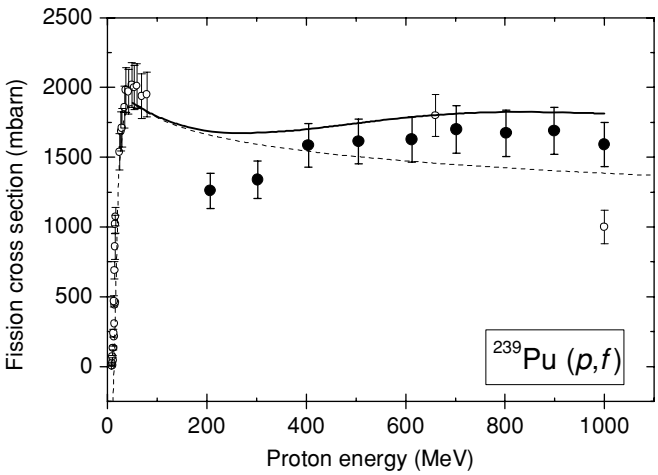

FIG. 7. Energy dependence of fission cross sections for ^{239}Pu. Solid circles, our data; open circles, data of previous experiments; dashed line, parametrization from Ref. [2]; solid line, the results of calculations in the framework of the cascade-evaporation model.

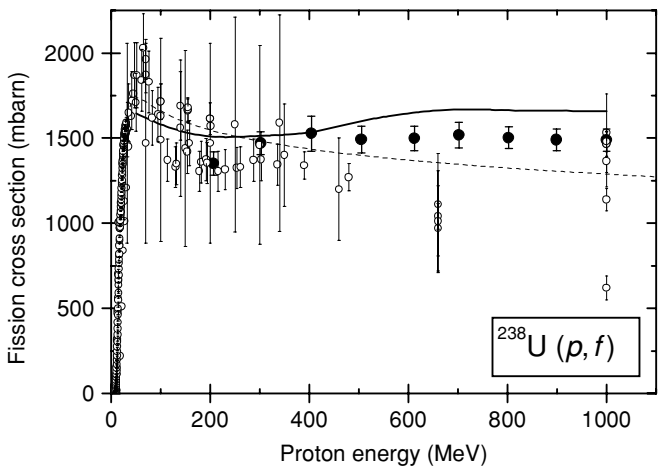

FIG. 9. Energy dependence of the fission cross sections for ^{238}U. Solid circles, our data; open circles, data from Refs. [2,3]; dashed line, a parametrization from Ref. [2]; solid line, theoretical calculation.

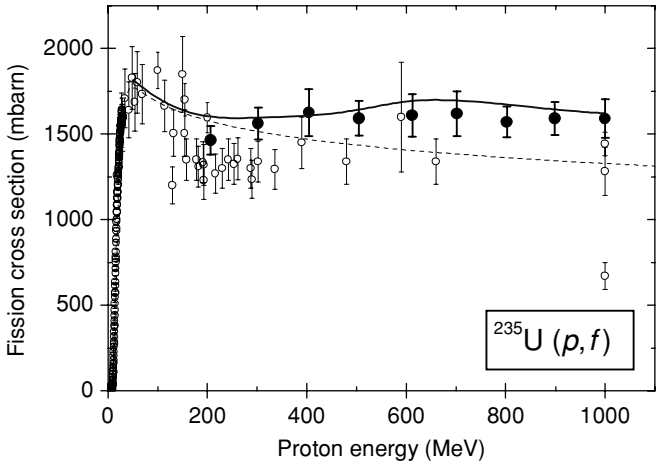

FIG. 10. Energy dependence of fission cross sections for ^{235}U. Solid circles, our data; open circles, data from Refs. [2,3]; dashed line, a parametrization from Ref. [2]; solid line, theoretical calculation.

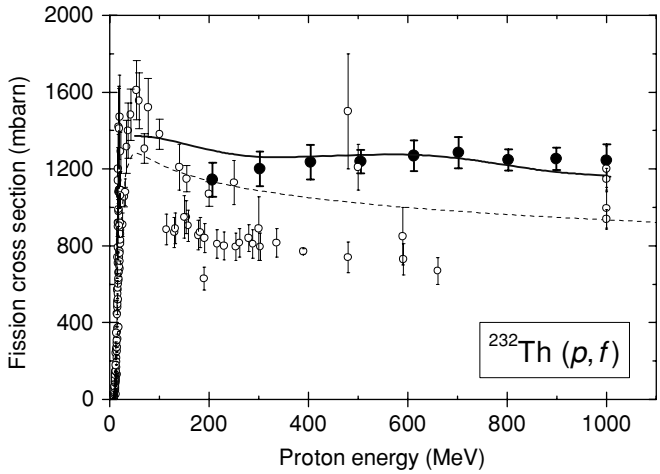

FIG. 12. Energy dependence of fission cross sections for ^{232}Th. Solid circles, our data; open circles, data from Refs. [2,3]; dashed line, a parametrization from Ref. [2]; solid line, theoretical calculation.

at 200 MeV, while for higher energies there is only occasional agreement with some of the experiments. The exception is the data for the ^{238}U nucleus, where our data at 1000 MeV are in a good agreement with the data of Refs. [19–21] as well as with the experimental data [22] obtained in the inverse kinematics in the reaction ^{238}U(1A GeV)+p.

As for the ^{232}Th target, our data demonstrate the approximate constancy of the cross sections for energies above 300 MeV, in agreement with the data of Ref. [17], where the fission fragments were detected in coincidence in the distant geometry which allowed accurate measurement of the angular correlations of the fragments. At the same time the majority of the previous data give much lower values for the fission cross sections in the energy range 100–700 MeV. One should note, however, that these data were obtained with the detection of a single fission fragment.

Our experimental results for actinide nuclei together with the previously available data at low energies (below 200–300 MeV) form a certain picture of the energy behavior of the fission cross sections in the whole energy range from the threshold up to 1000 MeV. In fact, a large body of the data indicate (at least for ^{237}Np, ^{238}U, ^{235}U, and ^{232}Th nuclei) the presence of the maximum in energy dependence near several tens of MeV, followed by the cross section decrease up to ∼200 MeV. Then after the indistinct minimum near 200–300 MeV the cross sections rise again up to ∼400 MeV, reaching a plateau which continues up to the maximum energy of 1000 MeV. The change in the energy behavior of the fission cross sections near 200 MeV resembles a characteristic minimum of the total inelastic cross section of the proton–nucleus interaction in the same energy region [23,24].

The energy behavior of the cross sections for pre-actinide nuclei ^{209}Bi and ^{nat}Pb (Figs. 13–14) demonstrates a sharp increase in the range 200–400 MeV, changing gradually to plateau at higher energy, at about 500 MeV for ^{209}Bi and ∼700 MeV for ^{nat}Pb. Our data for ^{209}Bi nuclei are in a good agreement with those of previous experiments in the

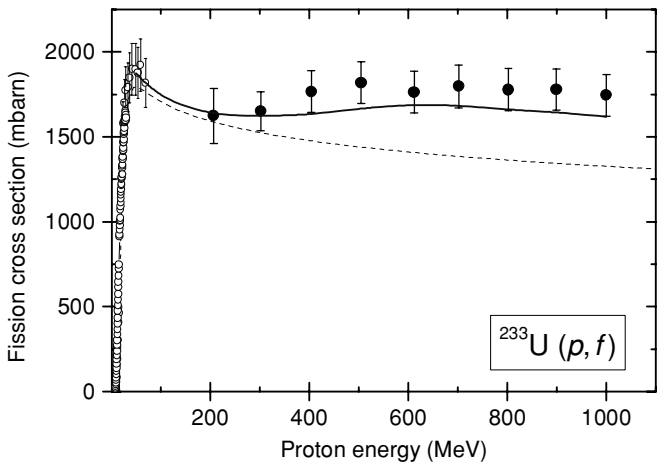

FIG. 11. Energy dependence of fission cross sections for ^{233}U. Solid circles, our data; open circles, data from Refs. [2,3]; dashed line, a parametrization from Ref. [2]; solid line, theoretical calculation.

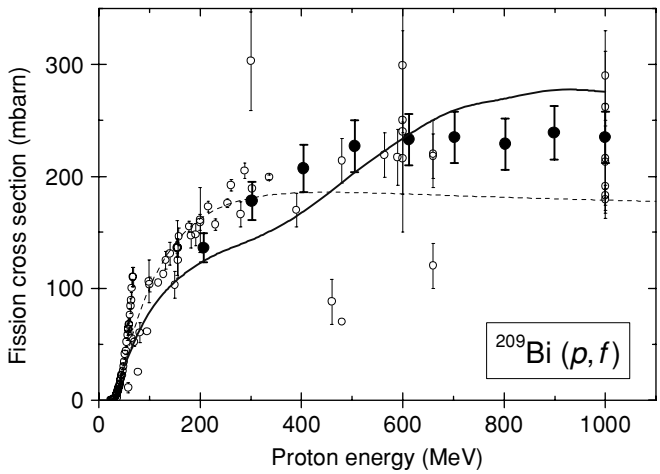

FIG. 13. Energy dependence of fission cross sections for ^{209}Bi. Solid circles, our data; open circles, data from Refs. [2,3]; dashed line, a parametrization from Ref. [2]; solid line, theoretical calculation.

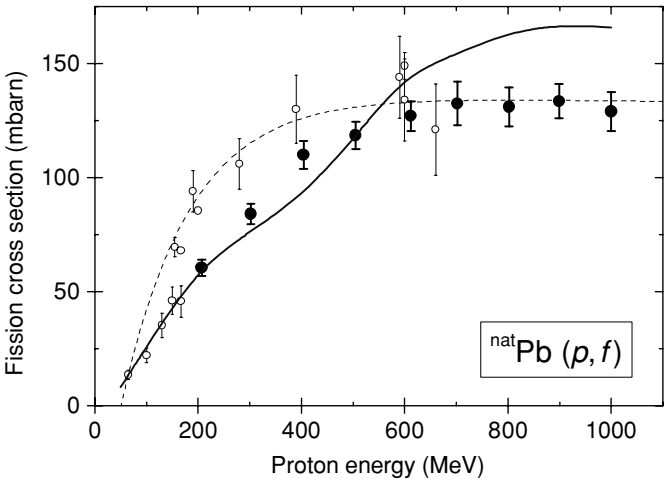

FIG. 14. Energy dependence of fission cross sections for ^{nat}Pb. Solid circles, our data; open circles, data from Refs. [2,3]; dashed line, a parametrization from Ref. [2]; solid line, theoretical calculation.

energy range 200–600 MeV, while for ^{nat}Pb our data in the range 200–400 MeV lie somewhat lower than the previous experimental results.

For ^{209}Bi the calculations of the cross sections with the help of parametrization [2], which took into account all the previous experimental data, give cross sections below those measured in the experiment for energies above 400 MeV. At the same time, for ^{nat}Pb the calculations [2] agree with our results except for some difference in the energy region 200–400 MeV.

Theoretically the heavy nuclei fission induced by nucleons of intermediate and high energy is traditionally analyzed in the framework of the two-step cascade evaporation model [25–27]. At the first stage of the reaction, when the mean range of the incident proton in the nucleus is comparable with or greater than the nucleus diameter, the interaction of the nucleon with the nucleus may be considered as a cascade of binary collisions of the incident nucleon with separate nucleons of the initial nucleus. During this fast stage ($\tau \sim 10^{-22}$ s) some part of the fast nucleons leaves the nucleus, taking away a considerable amount of energy. The rest of the energy is transformed into the excitation energy of the residual nucleus, whose nucleon composition differs from that of the initial nucleus. So, after the cascade stage of the reaction a residual nucleus appears with wide spectra of nucleon compositions and excitation energies, which depend on the incident nucleon energy. At the second (slow) stage of the reaction ($\tau \sim 10^{-16}$–10^{-19} s) the highly excited nucleus either emits nucleons or undergoes fission. The calculation of the cascade stage of the interaction was carried out by us with the help of the modified version of the model of the internuclear cascade [28], in which a Fermi-gas model of the nucleus was used taking into account the nucleon density spread at the border of the nucleus. This version of the cascade-evaporation model was successfully used earlier to analyze the reactions of deep disintegration [29,30] and fission [4] induced by 1-GeV protons. At the stage of decay of the highly excited nucleus the fission cross section is determined mainly by the ratio of the fission probability to the probability of the neutron emission [31]. The probability of the neutron emission was calculated in the frame of the statistical theory of Weisskopf [32], neutron emission probability being considered in the Bohr-Wheeler approach [33]. When calculating the fission cross sections, one needs, as a rule, to vary the nuclear level density at the equilibrium deformation a_n and at the saddle point of the fissioning nucleus a_f, as well as at the fission barrier value B_f. It was supposed that at high excitation energy nuclear shell effects in the fission barriers may be neglected, the ratio of the level density parameters a_f/a_n being supposed to be independent of the excitation energy of the decaying nucleus. In our calculations the level density parameter a_n was taken to be $A/10$ MeV^{-1} for all actinide nuclei. For the pre-actinide nuclei of Bi and Pb it was necessary to take into account the shell effects for calculation of the density parameter because these nuclei are in the vicinity of nucleon magic numbers. By taking these corrections into account, a value of the level density parameter for pre-actinide nuclei is $A/16$. The ratio of the level density parameters a_f/a_n being equal to 1.1 for pre-actinide and actinide nuclei. The fission barriers calculated in the liquid drop model [34] were used for B_f. The results of the calculations are presented by solid lines in Figs. 7–14. It is seen that the calculations reproduce qualitatively the general behavior of the cross sections in the range 50–1000 MeV, with a minimum near 200–300 MeV and a plateau above 400 MeV for actinide nuclei. However, our experimental data for ^{237}Np and ^{239}Pu (Figs. 7 and 8) at 200 and 300 MeV and for ^{nat}Pb at 700–1000 MeV (Fig. 14) lie considerably lower than the calculated cross sections.

The dependence of the total fission cross sections on the parameter Z^2/A of the target nucleus is shown in Fig. 15 for the cross sections from the saturation region (at a proton energy of 1000 MeV). It is seen that the total fission cross section is an increasing function of the Z^2/A parameter only up to ^{233}U, while for ^{237}Np and ^{239}Pu the cross sections are equal, but lower than that for ^{233}U. In addition, the fission cross sections for uranium isotopes in the whole energy range demonstrate systematically (despite considerable experimental uncertainties) the rise of

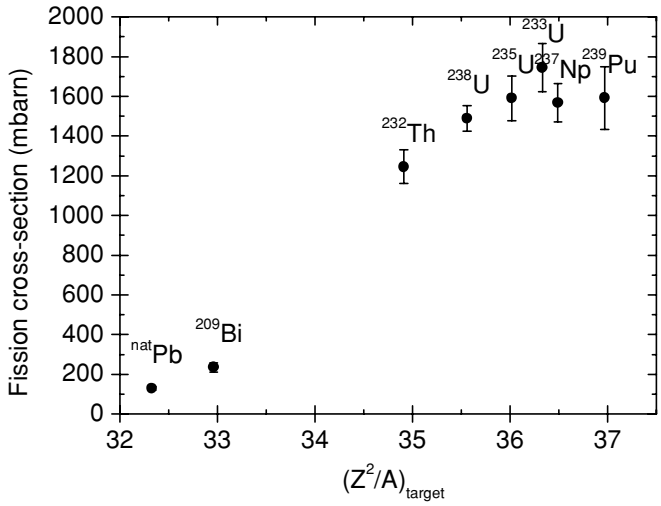

FIG. 15. Dependence of total fission cross sections on the parameter Z^2/A of the target nucleus.

the cross section when coming from ^{238}U to lighter isotopes. The isotope dependence of the fission cross sections for uranium was observed earlier in experiments on fission induced by neutrons [35,36] and γ photons [37] of intermediate energies. The cross section values for uranium fission induced by neutrons of 100–300 MeV are in a good agreement with our data in the corresponding energy region. However, the existence of isotope dependence of uranium fission cross sections for higher energies looks unexpected and strange from the viewpoint of the cascade-evaporation model for two reasons. First, as was previously stated, the result of the cascade stage of the proton–nucleus interaction is the formation of the wide isotope spectrum of the residual excited nuclei, which should lead to "loss of the memory" about the nucleon composition in the input channel of the reaction (nucleon composition of the initial nucleus). Second, the fission barriers B_f for the uranium nuclei calculated in the liquid drop model amount to less than 10 MeV [34], the difference in the B_f values for a series of residual nuclei not exceeding several MeV. Therefore the version of the cascade-evaporation model we used cannot reproduce the isotopic dependence of the fission cross sections for uranium nuclei.

IV. CONCLUSIONS

For the first time in the single experimental technique the cross sections of proton induced fission for ^{nat}Pb, ^{209}Bi, ^{232}Th, ^{233}U, ^{235}U, ^{238}U, ^{237}Np, and ^{239}Pu nuclei have been measured in the wide energy range from 200 to 1000 MeV. Analysis of the results and comparison with previous experimental data allow one to come to the following conclusions.

(i) The cross sections for all actinide nuclei have similar energy dependencies, characterized by the rise of the cross sections in the range from 200 to ~400 MeV, followed by a plateau, that continues up to at least 1000 MeV.

(ii) For pre-actinide nuclei Bi and Pb the increase of the cross sections for energies above 200 MeV is faster. The rise then changes to a plateau, which begins at ~500 MeV for ^{209}Bi and ~600 MeV for ^{nat}Pb and continues upto 1000 MeV.

(iii) The calculations of the fission cross sections in the framework of the cascade-evaporation model allow one to reproduce qualitatively the cross section behavior.

(iv) The data for uranium isotopes in the whole energy range demonstrate the systematic rise (despite considerable experimental uncertainties) of the cross section when coming from ^{238}U to lighter isotopes.

(v) The total fission cross section in the saturation region (at a proton energy of 1000 MeV) is an increasing function of the Z^2/A parameter only up to ^{233}U, while the cross section values for ^{237}Np and ^{239}Pu are approximately equal to the cross section values for ^{235}U.

ACKNOWLEDGMENTS

The authors are deeply grateful to A. A. Goverdovsky and A. V. Kravtsov for helpful discussions and to V. A. Mitrofanov for valuable help in target preparation. This work was financially supported by an ISTC grant in the frame of Project 1405.

[1] A. J. Koning, J.-P. Delaroche, and O. Bersillon, Nucl. Instrum. Methods Phys. Res. A **414**, 49 (1998).
[2] A. V. Prokofiev, Nucl. Instrum. Methods Phys. Res. A **463**, 557 (2001).
[3] A. I. Obukhov, Phys. Part. Nucl. **32**, 162 (2001).
[4] L. N. Andronenko, A. A. Kotov, M. M. Nesterov, V. F. Petrov, N. A. Tarasov, L. A. Vaishnene, and W. Neubert, Z. Phys. A **318**, 97 (1984).
[5] N. K. Abrosimov, V. G. Vovchenko, V. A. Eliseev, E. M. Ivanov, Yu. T. Mironov, G. A. Riabov, M. G. Tverskoy, and Yu. A. Chestnov, Report No. PNPI-2525, Petersburg Nuclear Physics Institute, 2003 (in Russian).
[6] GEANT–http://wwwasdoc.web.cern.ch/wwwasdoc/geant_html3/geantall.html.
[7] Yu. P. Gangrskiy, B. N. Markov, and V. P. Perelygin, *Registration and Spectrometry of Fission Fragments* (Energoatomizdat, Moscow, 1992) (in Russian).
[8] A. A. Kotov, W. Neubert, L. N. Andronenko, B. L. Gorshkov, G. G. Kovshevny, L. A. Vaishnene, and M. I. Yazikov, Nucl. Instrum. Methods **178**, 55 (1980).
[9] V. G. Vovchenko, L. A. Vaishnene, Yu. A. Gavrikov, A. A. Kotov, V. I. Murzin, V. V. Poliakov, S. I. Trush, O. Ya. Fedorov, Yu. A. Chestnov, A. V. Shvedchikov, and A. I. Chtchetkovski, Report No. PNPI-2532, Petersburg Nuclear Physics Institute, 2003 (in Russian).
[10] SRIM- http://www.srim.org
[11] L. C. Northcliffe and R. F. Schilling, Nucl. Data Tables A **7**, 233 (1970).
[12] J. Galin, M. Lefort, J. Peter, X. Tarrago, E. Cheifetz, and Z. Frankel, Nucl. Phys. **A134**, 513 (1969).
[13] A. A. Kotov, G. G. Semenchuk, L. N. Andronenko, M. N. Andronenko, B. L. Gorshkov, G. G. Kovshevny, V. R. Reznik, and G. E. Solyakin, Yad. Fiz. **20**, 467 (1974) (in Russian).
[14] L. Kowalski and C. Stephan, J. Phys. (Paris) **24**, 901 (1963).
[15] C. J. Stephan and M. L. Perlman, Phys. Rev. **164**, 1528 (1967).
[16] A. A. Kotov, G. G. Semenchuk, B. A. Bochagov, B. L. Gorshkov, G. G. Kovshevny, V. R. Reznik, and G. E. Solyakin, Yad. Fiz. **17**, 950 (1973) (in Russian).
[17] F. Saint-Laurent, M. Conjeaud, R. Dayras, S. Harar, H. Oeschler, and C. Volant, Nucl. Phys. **A422**, 307 (1984).
[18] V. I. Yurevich, V. A. Nikolaev, R. M. Yakovlev, and A. N. Sosnin, Yad. Fiz. **65**, 1417 (2002) (in Russian).
[19] L. A. Vaishnene, L. N. Andronenko, G. G. Kovshevny, A. A. Kotov, G. E. Solyakin, and W. Neubert, Z. Phys. A **302**, 143 (1981).
[20] B. A. Bochagov, V. S. Bychenkov, V. D. Dmitriev, S. P. Maltsev, A. I. Obukhov, N. A. Perfilov, V. A. Udod, and O. E. Shigaev, Yad. Fiz. **28**, 572 (1978) (in Russian).
[21] J. Hudis and S. Katcoff, Phys. Rev. C **13**, 1961 (1976).
[22] M. Bernas, P. Armbruster, J. Benlliure, A. Boudard, E. Casarejos, S. Czajkowski, T. Enqvist, R. Legrain, S. Leray, B. Mustapha, *et al.*, Nucl. Phys. **A725**, 213 (2003).

[23] F. S. Alsmiller, R. G. Alsmiller Jr., T. A. Gabriel, R. A. Lillie, and J. Barish, Nucl. Sci. Eng. **79**, 147 (1981).
[24] V. S. Barashenkov, Report No. JINR P2-89-770, 1989 (in Russian).
[25] R. Serber, Phys. Rev. **72**, 1114 (1947).
[26] V. S. Barashenkov and V. D. Toneyev, *Vzaimodejstvia visokoenergeticheskih chastits i atomnih yader s yadrami* (Atomizdat, Moscow, 1972) (in Russian).
[27] K. K. Gudima, S. G. Mashnik, and V. D. Toneev, Nucl. Phys. **A401**, 329 (1983).
[28] V. E. Bunakov, M. M. Nesterov, and N. A. Tarasov, Phys. Lett. **B73**, 267 (1978).
[29] L. H. Batist, E. N. Volnin, V. T. Grachev, A. M. Zolotov, A. A. Lobodenko, D. M. Seliverstov, N. N. Smirnov, and N. A. Tarasov, Leningrad Nuclear Physics Institute, Report No. LNPI–606, 1980 (in Russian).
[30] M. M. Nesterov and N. A. Tarasov, Leningrad Nuclear Physics Institute, Report No. LNPI-619, 1980 (in Russian).
[31] A. S. Iljinov, E. A. Cherepanov, and S. E. Chigrinov, Z. Phys. A **287**, 37 (1978).
[32] V. F. Weisskopf, Phys. Rev. **52**, 295 (1937).
[33] N. Bohr and J. A. Wheeler, Phys. Rev. **56**, 426 (1939).
[34] W. D. Myers and W. J. Swiatecki, Ark. Fys. **36**, 343 (1967).
[35] O. Shcherbakov, A. Donets, A. Evdokimov, A. Fomichev, T. Fukahori, A. Hasegava, A. Laptev, V. Maslov, G. Petrov, S. Soloviev, Yu. Tuboltsev, and A. Vorobyev, Journ. Nucl. Sci. and Techn., Proceedings. of International Conference. on Nuclear. Data for Sciences and Technologies, Tsukuba, Japan, Oct.7–12, 2001, Ed. K.Shibata, Atomic Energy Society of Japan, p. 230, 2002.
[36] P. W. Lisowski, A. Gavron, W. E. Parker, S. J. Balestrini, A. D. Carlson, O. A. Wasson, and N. W. Hill, Journ. Nucl. Sci. and Techn., Proceedings. of International Conference. on Nuclear. Data for Sciences and Technologies, Julich, Germany, May 13–17, 1991, Ed. S. M. Qaim, Springer-verlag, Berlin, Heidelberg, p. 732, 1992.
[37] J. C. Sanabria, B. L. Berman, C. Cetina, P. L. Cole, G. Feldman, N. R. Kolb, R. E. Pywell, J. M. Vogt, V. G. Nedorezov, A. S. Sudov, and G. Ya. Kezerashvili, Phys. Rev. C **61**, 034604 (2000).